Comparing spin injection in $Fe_{75}Co_{25}/Bi_2Te_3$ at GHz and optical excitations

Vinay Sharma[1], Rajeev Nepal[1], Weipeng Wu[2], E.A Pogue[3], Lars Gundlach[2,4], M. Benjamin Jungfleisch[2, *], Ramesh C. Budhani[1, *]

[1]Department of Physics, Morgan State University, Baltimore, Maryland 21210 USA

[2]Department of Physics and Astronomy, University of Delaware, Newark, DE 19716, USA

[3]Department of Chemistry, The Johns Hopkins University, Baltimore, Maryland 21218, USA

[4]Department of Chemistry and Biochemistry, University of Delaware, Newark, DE 19716, USA

***Corresponding authors:** mbj@udel.edu, Ramesh.budhani@morgan.edu

ABSTRACT

Spin-to-charge conversion (S2CC) processes in thin film heterostructures have attracted much attention in recent years. Here we describe the S2CC in a 3-D topological insulator Bi_2Te_3 interfaced with an epitaxial film of $Fe_{75}Co_{25}$. The quantification of spin-to-charge conversion is made with two complementary techniques: ferromagnetic resonance (FMR) based inverse spin Hall effect (ISHE) at GHz frequencies and femtosecond light-pulse induced emission of terahertz (THz) radiation. The role of spin rectification due to extrinsic effects like anisotropic magnetoresistance (AMR) and planar Hall effects (PHE) is pronounced at the GHz time scale, whereas the THz measurements do not show any detectible signal which could be attributed to AMR or PHE. This result may be due to (i) homodyne rectification at GHz, which is absent in THz measurements and (ii) laser-induced thermal spin-current generation and magnetic dipole radiation in THz measurements, which is completely absent in GHz range. The converted charge current has been analyzed using the spin diffusion model for the ISHE. We note that regardless of the differences in timescales, the spin diffusion length in the two cases is comparable. Our results aid in understanding the role of spin-pumping timescales in the generation of ISHE signals.

Introduction

The time-varying magnetization of a magnetically ordered material may pump pure spin current into a proximate non-magnetic layer [1-3]. This spin angular momentum transfer across the interface is stimulated by the excitations of varying timescales such as thermal gradients, microwaves, and optical radiation [4-9]. However, the strength and efficiency of this transfer are controlled by the robustness of magnetization and spin mixing conductance of the interface [10,11] respectively. The latter is affected strongly by the metallurgical and chemical characteristics of the interface between the non-magnetic metal (NM) and ferromagnet (FM) [12,13]. The leaking angular momentum, characterized by spin current density $\mathbf{j}_s$ enhances the Gilbert damping parameter of the precessing magnetization in the FM layer. The injected $\mathbf{j}_s$ into the NM layer converts into a charge current $\mathbf{j}_c$ through two different processes (i) bulk inverse spin Hall effect (ISHE), which is dominant when the thickness of the NM layer is greater than spin diffusion length (λ_{SD}), and (ii) symmetry breaking inverse Rashba Edelstein effect (IREE) in ultrathin Dirac materials [14-16]. The $\mathbf{j}_c$ eventually produces a dc voltage V_{dc} across the sample under open circuit conditions. The process of ISHE in heterostructures comprised of insulating ferrimagnets (FiM) and heavy metals is well-established [17]. However, for metallic FMs, this V_{dc} is contaminated by various spin rectification effects (SRE) like anisotropic magnetoresistance (AMR), anomalous Hall effect (AHE) and planar Hall effect (PHE) [18], thus obscuring the true ISHE contribution. The different sign of ISHE voltages in the same NM interfaced with FiM and metallic FMs require more understanding and discussion [19-21]. We expect that this contradiction will be pronounced in (i) the FMs with lower Gilbert damping due to the inverse dependence of j_s on the Gilbert damping parameter (α), (ii) in FMs with large anisotropic magneto-transport and (iii) in topological insulators (TIs) due to competing effects like the IREE. Few recent works report ultra-low Gilbert damping in polycrystalline and epitaxial films of $Fe_{75}Co_{25}$ [22-26]. The epitaxial Fe-Co alloys also display large AMR and PHE due to a strong *sd*-scattering near the Fermi energy [27-28]. A study of the frequency-dependence of AMR-based homodyne rectification over a broad frequency range, which may address the contributions of extrinsic and intrinsic effects to the dc voltage has its own merit.

In this paper, we address the spin-to-charge conversion (S2CC) processes at the interface of epitaxial $Fe_{75}Co_{25}$ thin films interfaced with the topological insulator Bi_2Te_3 by exciting the

magnetization of the former at two different time scales, namely: (1) through microwave radiation of frequency tuned to ferromagnetic resonance (FMR) in $Fe_{75}Co_{25}$, and (2) femtosecond laser-induced spin injection which leads to emission of THz radiation. We have addressed the roles of spin rectification through AMR, PHE and AHE in the measurements performed at GHz frequencies, whereas the THz emission is explained in the framework of laser induced thermal spin current generation, magnetic dipole radiation and ultrafast demagnetization.

The details of $Fe_{75}Co_{25}/Bi_2Te_3$ bilayer synthesis are given in the supplementary section. The thin films have been labeled as FC4 and FC4-BT2 to FC4-BT20 where FC and BT stand for $Fe_{75}Co_{25}$ and Bi_2Te_3 respectively and the numeral that follows FC and BT is the thickness of the respective layer in nm. The typical dimensions of the samples used for FMR-ISHE, and THz measurements are 7.0 x 2.0 mm^2 and 5.0 x 5.0 mm^2 respectively. Further details of the measurement setups are given in our previous works [6, 29-30]. Our results pave the way for the development of spintronic devices in a broad frequency range with a clear understanding of various spin excitation and rectification mechanisms.

The structural quality of the $Fe_{75}Co_{25}$ films has been established by X-ray diffraction (XRD) measurements performed in the Bragg-Brentano geometry. The equilibrium crystallographic structure of the $Fe_{75}Co_{25}$ alloy is a body-centered cubic (bcc) cell of lattice constant ≈ 2.85 Å [22]. Figure 1(a) shows the θ-2θ XRD pattern of the FC4 sample grown on the (001) surface of $MgAl_2O_4$ (MAO) single crystal wafers. The prominent (002) peak at 64.5^0 yields an out-of-plane lattice constant of ≈ 2.90 Å. The diffraction pattern also shows weak Laue oscillations which have been indicated by arrows in the figure. The inset of Fig. 1(a) is the rocking curve with a full width at half maximum of ≈ 0.19^0. The clear Laue oscillations and narrow rocking curve demonstrate epitaxial growth of $Fe_{75}Co_{25}$ on MAO (a = 8.083 Å) when we consider a 45^0 rotation of the basal plane of the bcc $Fe_{75}Co_{25}$ with respect to the basal plane of face-centered cubic MAO. Figure 1(b) shows the X-ray reflectivity (XRR) profile of FC4 sample. The modeling of these XRR data yields a film roughness of ≈ 0.3 nm. The crystallographic structure and surface roughness of FC4-BT20 sample are given in the supplementary file (Fig. S1). The crystallographic structure and electronic transport properties of the sputter deposited Bi_2Te_3 thin films have been reported elsewhere [31]. The temperature dependence of electrical resistivity and Hall coefficient of these films reveals a semi-metallic character of n-type conduction with carrier density and mobility of 12 x 10^{20}

electrons/cm^3 and 5 cm^2 V^{-1}s^{-1}, respectively [31]. The topological nature of Bi_2Te_3 electronic states is indicated by the presence of a robust planar Hall effect and anisotropic magnetoresistance due to tilting of Dirac cone by the in-plane magnetic field. [32, 33]. Our measurement on plain films of Bi_2Te_3 deposited on c-plane sapphire show a large anisotropy in in-plane field transport and this effect is dominant at T < 200 K [31]. However, in this work we are dealing with room temperature deposited Bi_2Te_3 films in which the topological surface states may not be well-defined and the transport may be dominated by the bulk states. Room temperature deposited Bi_2Te_3 films show a granular structure [31, 34] but their S2CC efficiency is comparable to that of films with high c-axis texture due to the possible quantum confinement in smaller crystallite grains [35].

Figure 1(c) shows the in-plane magnetization of FC4 and FC4-BT20 samples. The saturation magnetization in both cases reaches a value of $\mu_0 M_S \approx 1.65 \pm 0.2$ T with a coercivity of 20 mT. The saturation magnetization is lower by ≈ 20 % compared to the calculated value for the bcc $Fe_{75}Co_{25}$ [22, 23]. This discrepancy is presumably due to thin-film size effects [24] as the thickness of this film is only 4 nm. It is clear from Fig. 1(c) that the deposition of Bi_2Te_3 on $Fe_{75}Co_{25}$ does not affect the magnetization and coercivity of the latter significantly, suggesting the absence of any significant interdiffusion at the interface. Figure 1(d) shows the variation of magnetization of the FC4 film as the in-plane magnetic field is rotated from 0 to 360^0. The four-fold magnetic anisotropy seen in Fig. 1(d) confirms that the easy and hard axis (within the framework of in-plane cubic magnetic anisotropy) are along the [100] and [110] directions respectively.

Bi_2Te_3 is known to be a 3-D TI hence it is important to understand the different mechanisms of S2CC in this FM-TI interface. We have addressed this concern in supplementary file and reached a conclusion that ISHE is the dominant mechanism here. The method of measuring the S2CC described here is such that the spin current is excited in the FM and injected into the TI through the FM/TI interface. At GHz frequencies, we measure the dc voltage generated by ISHE across the TI layer (Fig. 2(a)). The symmetric dc signal (V_{symm}) produced in the FC4-BTx samples at 10 GHz excitation for an in-plane magnetic field is shown in Fig. 2(c). We note that the output dc voltage (V_{mix}) is derived from the superposition of symmetric and asymmetric Lorentizian functions [36]. We have extracted the overall ISHE and rectification responses by antisymmetrizing the signals obtained at the two polarities of the dc field. This procedure eliminates the possible contamination of the ISHE signal by thermal voltages. Supplementary Fig.

S2 shows the result of this procedure on sample FC4-BT2. This symmetrized data is fitted to the equation [36].

$$V_{mix} = K_s \frac{\delta H^2}{(H-H_r)^2+\delta H^2} + K_{as} \frac{-2\delta H(H-H_r)}{(H-H_r)^2+\delta H^2} \qquad (1)$$

Here, K_s and K_{as} are symmetric and asymmetric coefficients, and δH is the half-width at half maximum of the resonance. In Fig. 2(c) we show the symmetric component of the V_{mix} for all the samples. However, attributing this voltage entirely to ISHE may be erroneous because a dc voltage is also produced by rectification of the eddy currents in the metallic FM layer. This effect is clearly seen in the data of Fig. 2(c) for a plain film of $Fe_{75}Co_{25}$ (sample FC4) where we do not expect any ISHE contribution. The source of rectification seen here is the anisotropic electronic transport in the FM layer due to *s-d* scattering [18, 37]. The noteworthy feature of Fig. 2(c) is the drop in the dc voltage as Bi_2Te_3 is added on top of the $Fe_{75}Co_{25}$ layer, which suggests that the polarity of the true ISHE signal produced in the TI layer is opposite to that caused by the rectification of eddy currents in the FM layer. From this decreasing trend in the signal and the geometry of our experiment, and the relation $\boldsymbol{j_c} = \theta_{SH} (\boldsymbol{j_s} \times \boldsymbol{\sigma})$, we conclude that the spin Hall angle of these Bi_2Te_3 films has a positive sign, which is consistent with the reported data on Bi_2Te_3 exfoliated crystals [38].

In the time-domain THz spectroscopy measurements, the samples of varying Bi_2Te_3 layer thickness are excited by femtosecond pulses of a 800 nm wavelength laser beam with a repetition rate of 10 kHz (fluence ~ 0.8 mJ/cm^2, pulse width 35 fs). A mechanical chopper operating at 373 Hz is placed in the path of the pump beam to provide a reference signal for phase sensitive detection of THz emission. The femtosecond laser pulse is directed perpendicular to the plane of the sample while it sits in a ≈ 80 mT field, which aligns the magnetization of the $Fe_{75}Co_{25}$ film parallel to its plane. The emitted THz radiation is detected in a 1-mm-thick (110) ZnTe crystal by electro-optical sampling. All samples are measured in the time domain with a step size of 50 fs in air. Upon excitation by the femtosecond laser pulses, an ultrafast spin current $\mathbf{j}_S$ is generated in the $Fe_{75}Co_{25}$ [Fig. 2(b)], which transmits into the adjacent Bi_2Te_3 layer where it is converted into a charge current $\boldsymbol{j}_C$ by means of the ISHE. Subsequently, this charge current pulse gives rise to THz emission with a THz electric field $\boldsymbol{E}_{THz} \sim \partial \boldsymbol{j}_C/\partial t$ [39]. The time-domain traces of emission from different samples are shown in Fig. 2(d). As is obvious from the figure, there is a clear change of

the THz peak amplitude on varying the Bi_2Te_3 layer thickness. Various separation mechanisms and experiments have been done to eliminate THz response in bare Bi_2Te_3 and bare $Fe_{75}Co_{25}$ layer due to intrinsic effects, the details of which are given in supplementary file. (See supplementary Figure S3 and S4)

We also observe a clear change in the polarity of the ISHE and THz signals by reversing the direction of magnetic field [Fig. 3(a) and 3(b)]. This change in the sign of the signal is consistent with the vector relation between $\boldsymbol{j}_s$, $\boldsymbol{j}_c$ and the polarization $\boldsymbol{\sigma}$ of spin current. We have also symmetrized the ISHE and THz data of Fig. 3 to evaluate any contributions of thermal voltages generated by the likely heating effects of microwaves and femtosecond light pulses. The result of this procedure is shown in supplementary Fig. S5 (a). In the inset of supplementary Fig. S5(a), we also show that the differential signal of THz signals obtained for the two antiparallel magnetization alignments is negligibly small. The power-dependent ISHE voltage for FC4-BT2 sample shows a linear response in the power range of 0 dBm to +15 dBm (Supplementary Fig. S5(b)). All data shown in Fig. 2 and 3 have been collected in the linear response regime.

To quantify the spin diffusion length in Bi_2Te_3 using ISHE measurements, we first calculate the effective charge current in the TI layer by subtracting the symmetric peak voltage signal (V_{peak}) of bare FC4 from the corresponding symmetric voltage of FC4-BTx samples. The spin diffusion length of Bi_2Te_3 is estimated by the fitting of charge current ($I_C = V_{peak}/R_{TI}$) deduced from the symmetric voltage that corresponds to the ISHE signal using the following equation [6, 17],

$$I_c = \frac{V_{peak}}{R_{TI}} \propto \lambda_{SD}.\tanh\left(\frac{t_{Bi2Te3}}{2\lambda_{SD}}\right) \qquad (2)$$

Here, V_{peak}, R_{TI} and t_{Bi2Te3} are peak symmetric voltage, resistance of TI layer, and thickness of the Bi_2Te_3 bilayer respectively, and λ_{SD} is the spin-diffusion length. The I_c data and fit to Eq. 2 are shown in Fig. 4(a). The fitting yields a spin diffusion length λ_{SD} of 1.82 ± 0.76 nm which is comparable with the reported values in the similar bismuth-based topological insulators [35, 40-41]. This short spin-diffusion length suggests that the spin-polarized electronic charge current is mainly restricted to the bottom surface of our TI films, whose thickness is greater than 2 nm. The voltage generated due SRE in bare $Fe_{75}Co_{25}$ film is discussed in supplementary file where the contribution of AHE is minimal as evidenced by a very low Hall resistivity (See supplementary,

Fig. S6) whereas the AMR/PHE contribution is higher due to significant s-d scattering and topological band diagram [27].

We extract the spin relaxation length λ_{rel} (also called hot electron velocity) [42] of the ultrafast spin-polarized electron current in the Bi_2Te_3 layers. Figure 4(b) shows the normalized THz peak-to-peak amplitude extracted from the time-domain traces shown in Fig. 2(d) as a function of the Bi_2Te_3 layer thickness. The frequency-dependent THz electric field is given by the relation [42],

$$E_{THz}(\omega) = \frac{eZ_0}{n_{air}+n_{MAO}+Z_0G(w,t_{Bi2Te3})} J_c(\omega), \qquad (3) \text{ and}$$

where the $j_c(\omega)$ is expressed as

$$j_c(\omega) = \frac{AF_{inc}}{t_{FeCo}+t_{Bi2Te3}} j_s^0 . \lambda_{rel} \tanh\left(\frac{t_{Bi2Te3}}{2\lambda_{rel}}\right) . \gamma \qquad (4)$$

Here G, AF_{inc}, j_s^0 λ_{rel} and γ are conductance of bilayer, fraction of absorbed pump power, injected spin current density, relaxation length and spin Hall angle respectively. Under the approximation that these parameters are independent of TI layer thickness, we write the normalized THz field as [42]

$$\frac{E_{THz}}{E_{THz,max}} \approx \max\left(\frac{t_{FeCo}+t_{Bi2Te3}}{\tanh\left(\frac{t_{Bi2Te3}}{2\lambda_{rel}}\right)}\right) \frac{\tanh\left(\frac{t_{Bi2Te3}}{2\lambda_{rel}}\right)}{t_{FeCo}+t_{Bi2Te3}} \qquad (5)$$

Max in equation 5 is the maximum value of the function $\left(\frac{t_{FeCo}+t_{Bi2Te3}}{\tanh\left(\frac{t_{Bi2Te3}}{2\lambda_{rel}}\right)}\right)$ which is calculated by changing the different values of Bi_2Te_3 thickness. The solid line in Fig 4(b) is a fit to Eq. 5. It yields a relaxation length λ_{rel} of 2.03 ± 0.52 nm. This result agrees remarkably well with the spin diffusion length extracted from the ISHE measurements performed in the FMR mode at GHz frequencies. A recent report on GHz and THz spin transport mechanisms in antiferromagnets (AFMs) has identified a four-times larger spin propagation length at GHz frequencies compared to the THz frequency regime [43]. Therefore, Ref. [43] concluded that spin transport at THz frequencies is ballistic, whereas it is diffusive at GHz frequencies in the studied metallic heavy metal/antiferromagnet/ferromagnet system. In contrast, we find that the spin relaxation length is approximately the same at the two frequencies in our metallic ferromagnet/TI heterostructure, which suggests the same type of transport regime at GHz and THz frequencies. However, this

variation may arise due to the high frequency (THz) resonance in AFMs [44] which is absent in topological insulators. Previous reports on ultrafast spin-to-charge conversion processes in FM-TI heterostructures discussed the contribution of TSS and IREE effects [45, 46]. Wang et al. [45] performed a TI thickness-dependent S2CC measurements through THz generation in which non-tangent hyperbolic (tanh) and non-monotonic thickness dependence were attributed to the IREE process. However, in the current work, we have observed tanh thickness dependence which is a clear signature of bulk ISHE. Similarly, Rongione et al. [46] measured ultrafast S2CC current in Co-$SnBi_2Te_4$ multilayers where $SnBi_2Te_4$ was chosen over Bi_2Te_3 to avoid any contribution of bulk states.

There are two possible mechanisms which may contribute differently to the microwave and femtosecond optical responses leading to the dissimilar amplitude of FMR-ISHE and THz signals: (i) homodyne rectification in ISHE measurements due to the mixing of microwave signal with the magnetoresistance of FM layer at the resonance. It gives rise to a dc voltage with Lorentzian lineshape due to high AMR ratio and in-plane/out of plane rf magnetic field components present simultaneously in the co-planar waveguide [18]. This effect is generally absent in the THz experiment and (ii) diffusive ultrafast spin currents at the interface due to laser pumping in THz measurements. This process is absent in the FMR-ISHE experiment. Previous reports of THz generation in single metallic FM layers [6, 47-48] have mainly attributed to the contribution of AHE in amorphous FM layers which is a linear magneto-transport effect. In this work, we are dealing with highly crystalline $Fe_{75}Co_{25}$ film which has very low anomalous Hall resistivity (0.06 μΩ.cm) as confirmed in transport measurements shown in Fig. S6. We suspect that other effects such as SRE including AMR/PHE do not significantly contribute to the THz measurements as described above.

In summary, we fabricated bilayers of $Fe_{75}Co_{25}$ epitaxial films capped with polycrystalline Bi_2Te_3 in an ultrahigh vacuum sputtering system and characterized these bilayers using dc magneto-transport, spin pumping induced dc voltage measurements at FMR, and femtosecond light excitation. We find a clear spin pumping induced ISHE signal in our multilayer structures along with the dc voltage arising from high AMR ratio of $Fe_{75}Co_{25}$.The dissimilar sign and amplitude of FMR-ISHE and THz signals have been highlighted and discussed. Notwithstanding the different time scales, the extracted spin diffusion length from these two experiments is in close agreement.

Our results indicate that FMR induced spin pumping and ultrafast spin-current injection are promising complementary tools to investigate inverse spin Hall effect.

See the supplementary material for further details on the experiments.

Acknowledgments

The preparation of samples, followed by measurements of dc magnetization, FMR and ISHE were conducted at Morgan State University with support from the Air Force Office of Scientific research under grant # FA9550-19-1-0082. X-ray diffraction measurements were performed at the Johns Hopkins University, whereas ultrafast spectroscopy was done at the University of Delaware (UD). Research at UD was supported by NSF through the University of Delaware Materials Research Science and Engineering Center, DMR-2011824. M.B.J. acknowledges additional support from the NSF through Grant No. 1833000.

AUTHOR DECLARATIONS

Conflict of interest

The authors have no conflict of interest to disclose.

Author contributions

R.N. deposited the $Fe_{75}Co_{25}/Bi_2Te_3$ thin films and measured the DC magnetization, V.S. conducted the FMR and ISHE measurements, E.A.P. measured the structural characteristics of the films using XRD, W.W. conducted Terahertz measurements with support of L. G., M.B.J. and R.C.B. planned and formulated the scientific concept and supervised FMR and ISHE measurements. The paper was cowritten by V.S, M.B.J and R.C.B, with input from the rest of the authors.

.DATA AVAILABILITY

The data that support the findings of this study are available from the corresponding authors upon reasonable request.

REFERENCES

[1] Y. Tserkovnyak, A. Brataas, and G.E.W. Bauer, Phys. Rev. Lett. **88**, 117601 (2002).

[2] E. Šimánek and B. Heinrich, Phys. Rev. B **67**, 144418 (2003).

[3] I. Žutić, J. Fabian, and S. Das Sarma, Rev. Mod. Phys. **76**, 323 (2004).

[4] A. Brataas, B. van Wees, O. Klein, G. de Loubens, and M. Viret, Phys. Rep. **885**, 1 (2020).

[5] B.A. Ivanov, Low Temp. Phys. **45**, 935 (2019).

[6] V. Sharma, W. Wu, P. Bajracharya, D.Q. To, A. Johnson, A. Janotti, G.W. Bryant, L. Gundlach, M.B. Jungfleisch, and R.C. Budhani, Phys. Rev. Mater. **5**, 124410 (2021).

[7] K. Uchida, H. Adachi, T. Ota, H. Nakayama, S. Maekawa, and E. Saitoh, Appl. Phys. Lett. **97**, 172505 (2010).

[8] G. Siegel, M.C. Prestgard, S. Teng, and A. Tiwari, Sci. Rep. **4**, 4429 (2014).

[9] A. De, A. Ghosh, R. Mandal, S. Ogale, and S. Nair, Phys. Rev. Lett. **124**, 17203 (2020).

[10] J.E. Hirsch, Phys. Rev. Lett. **83**, 1834 (1999).

[11] M. Zwierzycki, Y. Tserkovnyak, P.J. Kelly, A. Brataas, and G.E.W. Bauer, Phys. Rev. B **71**, 64420 (2005).

[12] O. Mosendz, V. Vlaminck, J.E. Pearson, F.Y. Fradin, G.E.W. Bauer, S.D. Bader, and A. Hoffmann, Phys. Rev. B **82**, 214403 (2010).

[13] B.F. Miao, S.Y. Huang, D. Qu, and C.L. Chien, Phys. Rev. Lett. **111**, 66602 (2013).

[14] A. Manchon, H.C. Koo, J. Nitta, S.M. Frolov, and R.A. Duine, Nat. Mater. **14**, 871 (2015).

[15] M.B. Jungfleisch, Q. Zhang, W. Zhang, J.E. Pearson, R.D. Schaller, H. Wen, and A. Hoffmann, Phys. Rev. Lett. **120**, 207207 (2018).

[16] W. Zhang, M.B. Jungfleisch, W. Jiang, J.E. Pearson, and A. Hoffmann, J. Appl. Phys. **117**, 17C727 (2015).

[17] H.L. Wang, C.H. Du, Y. Pu, R. Adur, P.C. Hammel, and F.Y. Yang, Phys. Rev. Lett. **112**, 197201 (2014).

[18] M. Harder, Y. Gui, and C.-M. Hu, Phys. Rep. **661**, 1 (2016).

[19] A. Conca, B. Heinz, M.R. Schweizer, S. Keller, E.T. Papaioannou, and B. Hillebrands, Phys. Rev. B **95**, 174426 (2017).

[20] L. Mihalceanu, S. Keller, J. Greser, D. Karfaridis, K. Simeonidis, G. Vourlias, T. Kehagias, A. Conca, B. Hillebrands, and E.T. Papaioannou, Appl. Phys. Lett. **110**, 252406 (2017).

[21] D. Lee, D. Go, H.-J. Park, W. Jeong, H.-W. Ko, D. Yun, D. Jo, S. Lee, G. Go, J.H. Oh, K.-J. Kim, B.-G. Park, B.-C. Min, H.C. Koo, H.-W. Lee, O. Lee, and K.-J. Lee, Nat. Commun. **12**, 6710 (2021).

[22] M.A.W. Schoen, D. Thonig, M.L. Schneider, T.J. Silva, H.T. Nembach, O. Eriksson, O. Karis, and J.M. Shaw, Nat. Phys. **12**, 839 (2016).

[23] A.J. Lee, J.T. Brangham, Y. Cheng, S.P. White, W.T. Ruane, B.D. Esser, D.W. McComb, P.C. Hammel, and F. Yang, Nat. Commun. **8**, 234 (2017).

[24] Y. Cheng, A.J. Lee, J.T. Brangham, S.P. White, W.T. Ruane, P.C. Hammel, and F. Yang, Appl. Phys. Lett. **113**, 262403 (2018).

[25] L. Flacke, L. Liensberger, M. Althammer, H. Huebl, S. Geprägs, K. Schultheiss, A. Buzdakov, T. Hula, H. Schultheiss, E.R.J. Edwards, H.T. Nembach, J.M. Shaw, R. Gross, and M. Weiler, Appl. Phys. Lett. **115**, 122402 (2019).

[26] E.R.J. Edwards, H.T. Nembach, and J.M. Shaw, Phys. Rev. Appl. **11**, 54036 (2019).

[27] F.L. Zeng, Z.Y. Ren, Y. Li, J.Y. Zeng, M.W. Jia, J. Miao, A. Hoffmann, W. Zhang, Y.Z. Wu, and Z. Yuan, Phys. Rev. Lett. **125**, 97201 (2020).

[28] F. Zeng, X. Shen, Y. Li, Z. Yuan, W. Zhang, and Y. Wu, New J. Phys. **22**, 93047 (2020).

[29] P. Bajracharya, V. Sharma, A. Johnson, and R.C. Budhani, J. Phys. D. Appl. Phys. **55**, 75303 (2021).

[30] V. Sharma, P. Bajracharya, A. Johnson, and R.C. Budhani, AIP Adv. **12**, 35028 (2022).

[31] Rajeev Nepal, Vinay Sharma, Lisa Pogue, and Ramesh C. Budhani, Disorder driven variations in orbital magnetoresistance and planar Hall effect in Bi_2Te_3 thin films. Submitted (2022).

[32] A.A. Taskin, H.F. Legg, F. Yang, S. Sasaki, Y. Kanai, K. Matsumoto, A. Rosch, and Y. Ando, Nat. Commun. **8**, 1340 (2017).

[33] S.-H. Zheng, H.-J. Duan, J.-K. Wang, J.-Y. Li, M.-X. Deng, and R.-Q. Wang, Phys. Rev. B **101**, 41408 (2020).

[34] N. Bhattacharjee, K. Mahalingam, A. Fedorko, A. Will-Cole, J. Ryu, M. Page, M. McConney, H. Fang, D. Heiman, and N.X. Sun, (2022).

[35] M. DC, R. Grassi, J.-Y. Chen, M. Jamali, D. Reifsnyder Hickey, D. Zhang, Z. Zhao, H. Li, P. Quarterman, Y. Lv, M. Li, A. Manchon, K.A. Mkhoyan, T. Low, and J.-P. Wang, Nat. Mater. **17**, 800 (2018).

[36] K. Ando, S. Takahashi, J. Ieda, Y. Kajiwara, H. Nakayama, T. Yoshino, K. Harii, Y. Fujikawa, M. Matsuo, S. Maekawa, and E. Saitoh, J. Appl. Phys. **109**, 103913 (2011)

[37] T. McGuire and R. Potter, IEEE Trans. Magn. **11**, 1018 (1975).

[38] H. Wu, P. Zhang, P. Deng, Q. Lan, Q. Pan, S.A. Razavi, X. Che, L. Huang, B. Dai, K. Wong, X. Han, and K.L. Wang, Phys. Rev. Lett. **123**, 207205 (2019).

[39] W. Wu, C. Yaw Ameyaw, M.F. Doty, and M.B. Jungfleisch, J. Appl. Phys. **130**, 91101 (2021).

[40] H. Wang, J. Kally, J.S. Lee, T. Liu, H. Chang, D.R. Hickey, K.A. Mkhoyan, M. Wu, A. Richardella, and N. Samarth, Phys. Rev. Lett. **117**, 76601 (2016).

[41] O. V Yazyev, J.E. Moore, and S.G. Louie, Phys. Rev. Lett. **105**, 266806 (2010).

[42] T. Seifert, S. Jaiswal, U. Martens, J. Hannegan, L. Braun, P. Maldonado, F. Freimuth, A.

Kronenberg, J. Henrizi, I. Radu, E. Beaurepaire, Y. Mokrousov, P.M. Oppeneer, M. Jourdan, G. Jakob, D. Turchinovich, L.M. Hayden, M. Wolf, M. Münzenberg, M. Kläui, and T. Kampfrath, Nat. Photonics **10**, 483 (2016).

[43] O. Gueckstock, R.L. Seeger, T.S. Seifert, S. Auffret, S. Gambarelli, J.N. Kirchhof, K.I. Bolotin, V. Baltz, T. Kampfrath, and L. Nádvorník, Appl. Phys. Lett. **120**, 62408 (2022).

[44] A. Kirilyuk, A. V Kimel, and T. Rasing, Rev. Mod. Phys. **82**, 2731 (2010).

[45] X. Wang, L. Cheng, D. Zhu, Y. Wu, M. Chen, Y. Wang, D. Zhao, C.B. Boothroyd, Y.M. Lam, J.-X. Zhu, M. Battiato, J.C.W. Song, H. Yang, and E.E.M. Chia, Adv. Mater. **30**, 1802356 (2018).

[46] E. Rongione, S. Fragkos, L. Baringthon, J. Hawecker, E. Xenogiannopoulou, P. Tsipas, C. Song, M. Mičica, J. Mangeney, J. Tignon, T. Boulier, N. Reyren, R. Lebrun, J.-M. George, P. Le Fèvre, S. Dhillon, A. Dimoulas, and H. Jaffrès, Adv. Opt. Mater. **10**, 2102061 (2022).

[47] Q. Zhang, Z. Luo, H. Li, Y. Yang, X. Zhang, and Y. Wu, Phys. Rev. Appl. **12**, 54027 (2019).

[48] Y. Liu, H. Cheng, Y. Xu, P. Vallobra, S. Eimer, X. Zhang, X. Wu, T. Nie, and W. Zhao, Phys. Rev. B **104**, 64419 (2021).

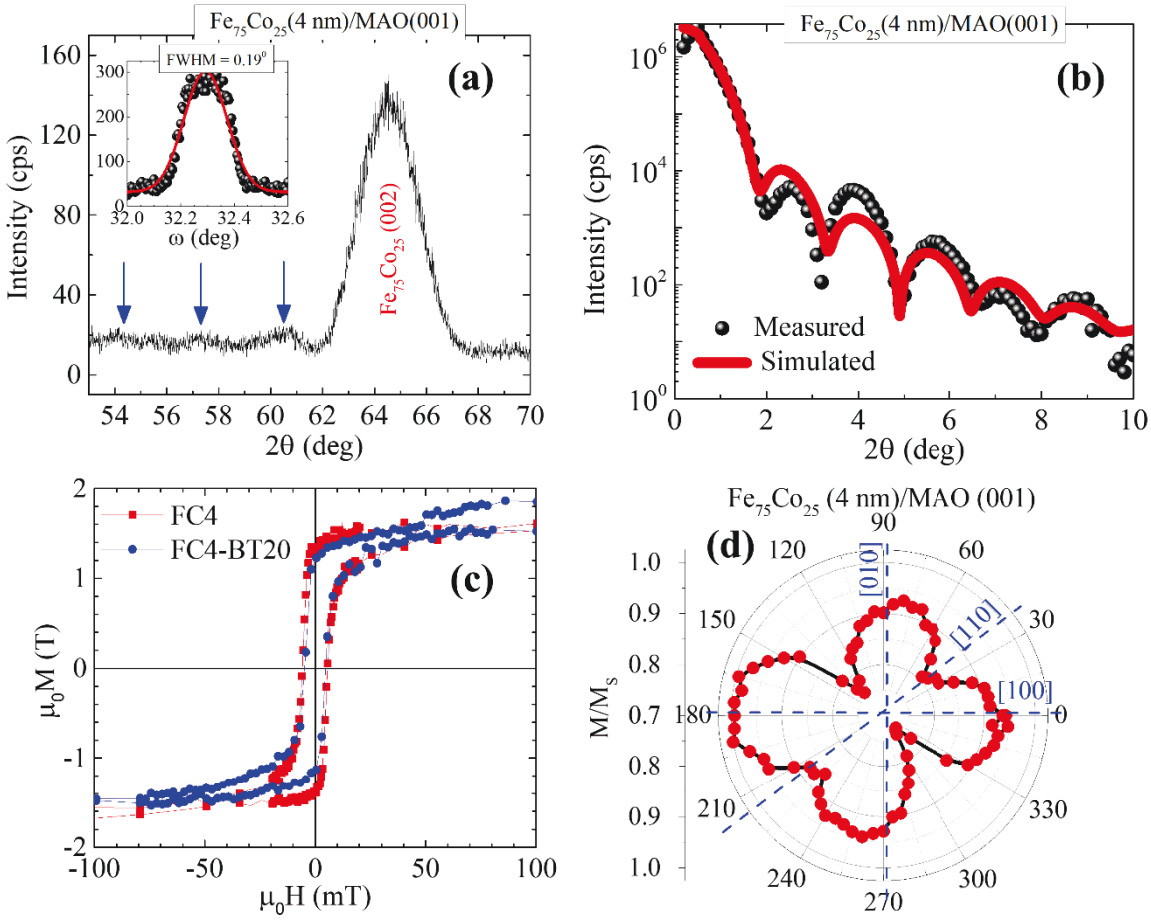

Figure 1 (a) θ-2θ X-ray diffraction pattern of FC4 sample on MAO (001) substrate. Inset shows the XRD rocking curve of $Fe_{75}Co_{25}$ (002) peak which has a full width at half maxima of 0.19^0. Arrows in the figure indicate the positions of Laue oscillations. (b) X-ray reflectivity scan of FC4 sample gives a surface roughness of 0.3 nm. (c) Magnetic hysteresis loops of FC4 and FC4-BT20 samples measured at room temperature with in-plane magnetic field. (d) The in-plane angular dependence of M/M_S for FC4 sample when the magnetic field is rotated from 0 to 360 degrees.

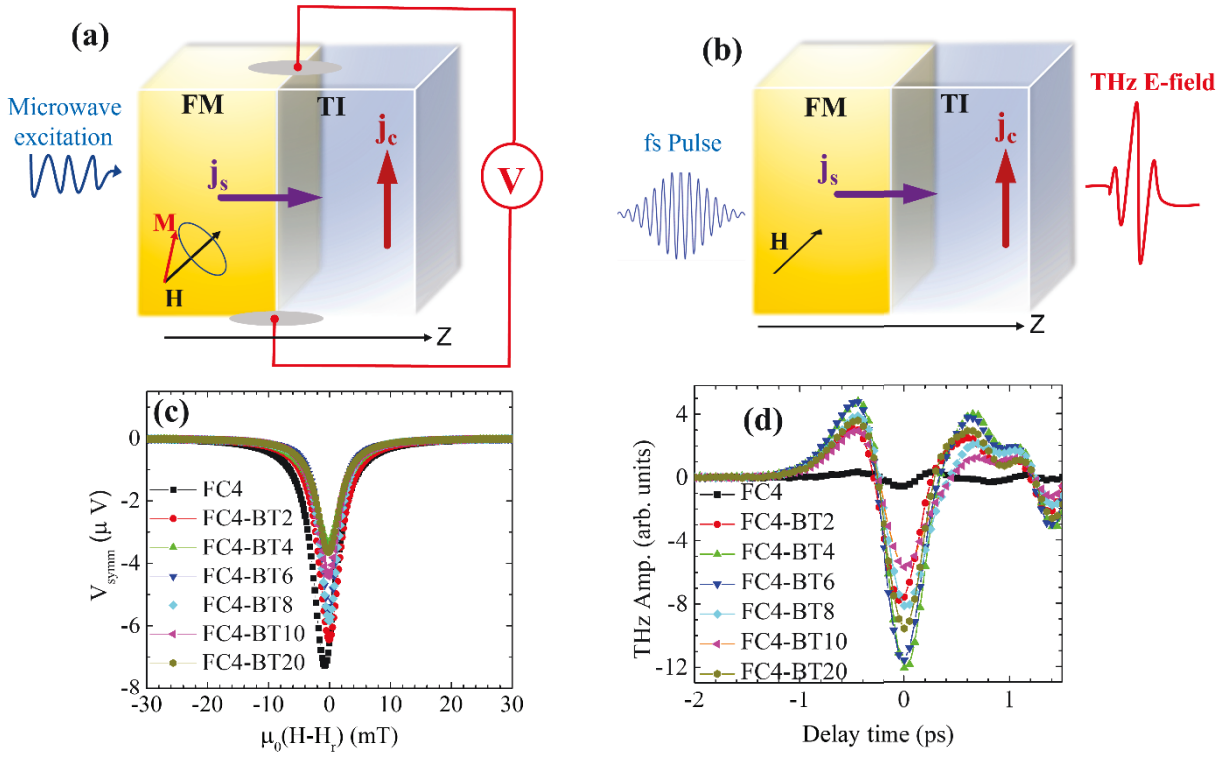

Figure 2 (a) Schematic of GHz ISHE experiment. An RF excitation of 10 GHz with h_{rf} = 0.02 mT excites the magnetization dynamics in the FM layer and injects a spin current into the NM. (b) Schematic of THz experiment where a fs light pulse excites spin precession and injects a spin current through the FM/NM interface to generate THz electric field. The THz electric field is polarized perpendicularly to the magnetization. (c) The ISHE related Symmetric component of dc voltage for bilayers of different Bi_2Te_3 layer thickness. (d) THz emission from $Fe_{75}Co_{25}/Bi_2Te_3$ bilayer films. The time traces are obtained using the time-domain THz spectroscopy system with a magnetic field applied in the plane of the bilayer.

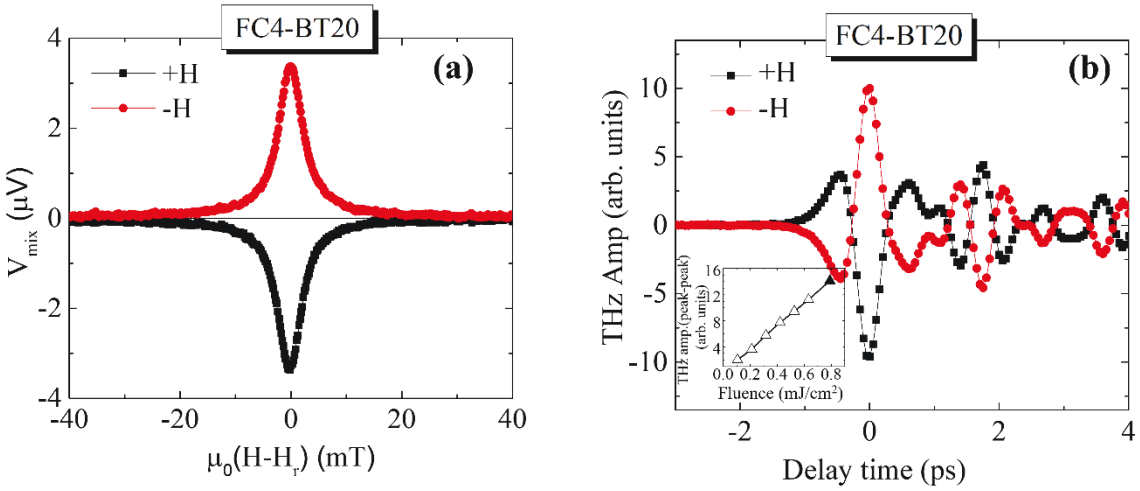

Figure 3 (a) ISHE signal for opposite polarities of magnetic field for the sample FC4-BT20, (b) THz signal for opposite polarities of magnetic field = 80 mT for the sample FC4-BT20. Inset shows the fluence dependence THz generation in linear region.

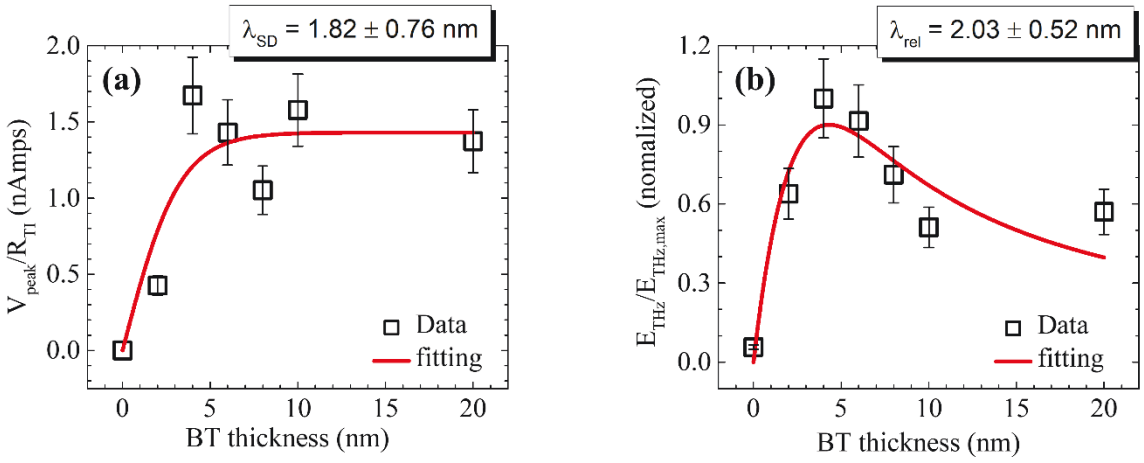

Figure 4 (a) ISHE induced charge current normalized by sample width plotted as a function of Bi_2Te_3 layer thickness. Solid line is a fit of these data to Eq. 2, which yields the spin diffusion length $\lambda_{SD} = 1.82 \pm 0.76$ nm in Bi_2Te_3. (b) Normalized THz electric field as a function of Bi_2Te_3 layer thickness, data is fitted with Eq. 5 to yield $\lambda_{rel} = 2.03 \pm 0.52$ nm.